Article

Kinetic Analysis of the Decomposition of the KFe$_3$(SO$_4$)$_{2-x}$(CrO$_4$)$_x$(OH)$_6$ Jarosite Solid Solution in Ca(OH)$_2$ Medium

Ister Mireles,[a] Iván A. Reyes,[*,b,c] Víctor H. Flores,[d] Francisco Patiño,[e] Mizraim U. Flores,[d,f] Martín Reyes,[a] Manuel Acosta,[g] Roel Cruz[b] and Emmanuel J. Gutiérrez[b,c]*

[a]*Área Académica de Ciencias de la Tierra y Materiales, Universidad Autónoma del Estado de Hidalgo, 42183 Mineral de la Reforma Hidalgo-HI, Mexico*

[b]*Instituto de Metalurgia, Universidad Autónoma de San Luis Potosí, 78210 San Luis Potosí-SL, Mexico*

[c]*Catedratico CONACyT - Consejo Nacional de Ciencia y Tecnología, Colonia Crédito Constructor Del. Benito Juárez, 03940 México-DF, Mexico*

[d]*Escuela Superior de Ingeniería Química e Industrias Extractivas, Instituto Politécnico Nacional, Unidad Profesional Adolfo López Mateos, 07738 México-DF, Mexico*

[e]*Ingeniería en Energía, Universidad Politécnica Metropolitana de Hidalgo, 43860 Tolcayuca-HI, Mexico*

[f]*Área de Electromecánica Industrial, Universidad Tecnológica de Tulancingo, 43642 Tulancingo-HI, Mexico*

[g]*División Académica de Ciencias Básicas, Universidad Juárez Autónoma de Tabasco, 86690 Cunduacán-TB, Mexico*

The decomposition of the solid solution of potassium jarosite with chromium(VI) in Ca(OH)$_2$ media was studied in the present work. According to experimental results, the incorporation of CrO$_4^{2-}$ into the crystal structure of jarosite resulted in a solid solution with the following approximate formula: [K$_{0.86}$(H$_3$O)$_{0.14}$]Fe$_{2.67}$[(SO$_4$)$_{1.23}$(CrO$_4$)$_{0.77}$][(OH)$_{5.01}$(H$_2$O)$_{0.99}$]. The experimental data describe a reaction based on the shrinking core model with chemical control for spherical particles. A reaction order of n = 0.67 and an activation energy (E$_a$) of 63.75 kJ mol^{-1} were obtained in the induction period (t$_{ind}$). The progressive conversion period is characterized by the diffusion of K$^+$, SO$_4^{2-}$ and CrO$_4^{2-}$ ions into the solution. In this stage, n = 1.99 with respect to OH$^-$, and E$_a$ = 51.56 kJ mol^{-1}. The CrO$_4^{2-}$ diffusion is slower compared to that of sulfate, a slight amount of chromate is adsorbed in the layer of the solid residue consisting on Fe(OH)$_3$. Finally, the equations that satisfactorily describe the reaction process were established from the data obtained.

Keywords: jarosite, chromate ion, solid solution, dissolution rates, kinetics analysis

Introduction

Chromium is one of the most important elements in the world and it is widely used in the chemical and metal industries. The toxicity of chromium has been a matter of interest in several industrialized countries. The sources of anthropogenic contamination include: fuel and carbon burning, production of ferrochrome, chromate, steels containing chromium, fungicides, cement, pigments, catalysis and oxidizers. Metal coating, leather tanning and oil drilling have increased this kind of pollution.[1] This kind of industrial and mining activities are the main source of chromium(VI) release into the environment.[2] The recent public concern regarding chromium(VI) in drinking water has boosted the research on technologies with potential to remove it from drinking water.[3]

Chromium can appear in different oxidation states, for instance chromium(VI), which is a carcinogen and potential pollutant agent. Water wells and water distribution systems are also affected by chromium(VI), so the pollution problem

*e-mail: iareyesdo@conacyt.mx, ivanalejandro2001@hotmail.com

posed by this metal has a great significance worldwide. The main chromium(VI) species are the chromate (CrO_4^{2-}) and dichromate ($Cr_2O_7^{2-}$) ions, which are quite soluble at any pH level affecting its mobility and transport of chromium. Chromium(VI) may be leached from the soil and penetrate phreatic zones; it can become a part of an aquifer and even migrate into surface water.[4] Due to the potential hazards to human health, there is a growing interest in understanding the process controlling the mobility of chromium(VI) in the environment. This, in order to assess the risks associated with released chromium and to design effective measures to clean the polluted sites. A key issue in the process that affects the mobility of chromium in the surface is the precipitation of solid phases containing chromium.[5]

Throughout the years, attempts have been made to design more efficient systems of remediation for polluted water containing heavy metals. Some methods have been studied to control and reduce contamination by chromium(VI) in water and soil, including residual biomass from tanneries to remove chromium(VI),[6] removal by biomaterials,[7] bioremediation,[8-12] reduction of chromium(VI) to chromium(III),[13] use of residual organic adsorbents,[14] and electrochemical treatments.[15] Among the existing alternatives for the removal of chromium(VI), there can be found minerals such as goethite, schwertmannite and jarosite. Jarosite-type compounds have proved to be better adsorbents compared to other minerals in the removal of dangerous metals, such as arsenic.[16] Since different ions can be incorporated into the jarosite structure, their precipitation has been used as a method to concentrate metals in solution. Its solubility depends on the pH and, therefore, jarosite dissolution is of great importance when controlling the mobility of trace elements adhered to its structure.[17]

Jarosite belongs to the isostructural group jarosite-alunite, which has a general formula $AB_3(ZO_4)_2(OH)_6$. Site A usually contains monovalent or divalent cations with a coordination number equal to or higher than 9,[18] with most of the ions in site A being K^+, Na^+ and H_3O^+;[19,20] however, Pb^{2+}, Ca^{2+} and NH_4^+ can also be incorporated.[21] Site B, octahedrally coordinated, in which solid substitutions are not commonly complete, is filled by Fe^{3+} in the jarosite group, and Al^{3+} in the alunite group,[22] but this site may also be partially substituted by Cr^{3+}, V^{3+} and Ga^{3+}. Site Z is tetrahedrally coordinated, with SO_4^{2-} being the dominant ion in jarosites and alunites; however, partial substitutions by PO_4^{2-}, AsO_4^{3-}, CO_3^{2-}, SbO_4^{2-}, CrO_4^{2-}, SiO_4^{4-} and SeO_4^{2-} have been reported.[23-25] The stability and reactivity of the jarosite mineral group depend on the substitution degree of other ions in sites A, B and on the tetrahedrons. The substitutions may result in an unbalance of the local charges and distort the lattice, thus introducing variations

in the free energy, which have an influence on the mineral's stability. Jarosites remain stable at highly acid and oxidizing conditions.[26] Several substitutions have been reported showing the flexibility of the jarosite structure towards the ion size and the charge arrangement. This characteristic makes minerals such as jarosite ideal to incorporate undesirable metallic elements that are also potentially dangerous for the environment.[27] The ion substitutions that alter the parameters of the unit cell of the ideal jarosite have been shown regarding the influence of dissolution and solubility rates. The substitution of H_3O and Na in site A significantly increases the jarosite solubility compared to jarosite with K, while the substitution of chromate by sulfate decreases the solubility of potassium jarosite.[5,22]

The most widespread method used to mitigate acid effluents is an active treatment process involving addition of a chemical-neutralizing agent, being lime the most common used agent. Addition of lime to acid mine drainage (AMD) raises its pH, accelerates the rate of chemical oxidation of ferrous iron and causes precipitation of metals present as hydroxides and carbonates.[28,29] For this reason, it is important to know the behavior of the phases that may contain elements of environmental importance, such as chromium(VI) in their structure, produced from $Ca(OH)_2$ under alkaline conditions. Understanding the dissolution reactions of such phases is notably important for an environmental assessment (for water and soil), since some of these elements could either return to the environment after being subjected to a mitigation process with a chemical-neutralizing agent. Although several studies have been conducted in $KFe_3(SO_4)_2(OH)_6$ and $KFe_3(CrO_4)_x(OH)_6$ solid solutions, there are no kinetic studies related to the decomposition of $KFe_3(SO_4)_{2-x}(CrO_4)_x(OH)_6$ in $Ca(OH)_2$ medium. In the present investigation, it was decided to incorporate chromium(VI) into the potassium jarosite since it is the most common phase in continental soil environments with enriched K, including AMD sediments and acid soil systems. Hydronium jarosite was synthesized in laboratory, although it is important to mention that its presence is not commonly observed in natural samples, which suggests that in normal soil conditions, sodium and potassium jarosites are the most stable phases that could be preserved at geological time scale.[30] Therefore, the aim of this study is to provide information regarding the stability of the $KFe_3(SO_4)_{2-x}(CrO_4)_x(OH)_6$ solid solution in $Ca(OH)_2$ medium, as well as its nature and kinetics. The effects of variables, such as concentration of anion hydroxide ($[OH^-]$), temperature (T) and particle size (d_0), were studied to determine the reaction order and activation energy to provide a kinetic model that allows describing the behavior of the decomposition reaction in $Ca(OH)_2$ medium, which

in turn will allow obtaining information about the stability of this compound under extreme alkalinity and temperature conditions.

Experimental

Synthesis

For the two syntheses performed, a procedure similar to that reported in previous works was followed;[31-36] the conditions are specified in Table 1. Iron(III) sulfate *n*-hydrate, $\geq 73\%$ as Fe$_2$(SO$_4$)$_3$, anhydrous potassium sulfate (99%), potassium chromate ($\geq 99\%$), iron(III) nitrate 9-hydrate ($\geq 98\%$), calcium hydroxide ($\geq 95\%$) and sulfuric acid (98%) were used, all in ACS grade (J. T. Baker, Tokyo, Japan). Salts that promote the formation of jarosite-type compounds were mixed in a 0.5 L of distilled water (26 MΩ cm) using a reactor (Pyrex, Corning Incorporated, Corning Inc., NY, USA) with a capacity of 1 L. A solution of 0.2 mol L^{-1} of dissolved K$_2$CrO$_4$ was prepared in a 100 mL volumetric flask (Pyrex, Corning Incorporated, Corning Inc., NY, USA) and then added to the reactor at a rate of 25 mL h^{-1}. A mechanical stirrer with a three blade propeller (IKA-RW 16 basic, IKA Works, Inc., Wilmington, NC, USA) was used at a stirring rate of 500 min^{-1} to keep the jarosite precipitates in suspension and promote faster crystal growth. The reactor was placed on a heating plate at 94 °C (Barnstead Thermolyne Super-Nuova, Thermo Fisher Scientific, Waltham, MA, USA) and coupled to a spiral condenser to make water circulate as a cooling fluid. The total time for the synthesis was 24 h. The obtained solids were vacuum-filtered with Whatman quantitative filter paper, grade 40 (Sigma-Aldrich, St. Louis, MO, USA) and repeatedly washed with hot (ca. 60 °C) distilled water to remove excess of K$^+$, Fe^{3+}, SO$_4^{2-}$ and CrO$_4^{2-}$. Then, they were dried in a furnace at 60 °C for 8 h. The same conditions used for the first synthesis, without adding K$_2$CrO$_4$, were used for the KFe$_3$(SO$_4$)$_2$(OH)$_6$ synthesis.

Characterization of precipitates

The granulometric characterization was conducted with series of Tyler test sieves (according to ASTM E11 - 13 Standard Specifications for Woven Wire Test Sieve Cloth and Test Sieves)[37] using mesh numbers 120 (d$_0 \geq 125$ μm), 170 (125 < d$_0 \geq 90$ μm), 200 (90 < d$_0 \geq 75$ μm), 270 (75 < d$_0 \geq 53$ μm), 325 (53 < d$_0 \geq 44$ μm), 400 (44 < d$_0 \geq 38$) and 500 (38 < d$_0 \geq 25$ μm). For the chemical analysis, 1 g of the solid solution KFe$_3$(SO$_4$)$_{2-x}$(CrO$_4$)$_x$(OH)$_6$ was dissolved in a solution of 20 mL H$_2$O + 20 mL HCl. Atomic absorption spectrometry (AAS, AAnalyst 200, PerkinElmer, Waltham, MA, USA) was used to determine Fe, K and Cr, while gravimetric analysis were carried out to determine SO$_4^{2-}$ as BaSO$_4$. Both syntheses were characterized by scanning electron microscopy (SEM, JEOL JSM-5900LV, JEOL USA, Inc., Peabody, MA, USA) with a coupled energy dispersive X-ray spectrometer (EDS, INCA X-Sight Model, Oxford Instruments plc, Abingdon, UK), and X-ray diffraction (XRD, Siemens D500, Siemens AG, Munich, Germany) using Cu Kα radiation (1.54056 Å) with a scanning step of 0.02° s^{-1}.

Decomposition experiments in Ca(OH)$_2$ medium

The decomposition experiments of KFe$_3$(SO$_4$)$_{2-x}$(CrO$_4$)$_x$(OH)$_6$ solid solution were conducted in a 1 L glass reactor. Different solution concentrations were prepared by stirring Ca(OH)$_2$ in a volumetric flask; the stirring time was 3 h and the highest concentration used was 1.4 g L^{-1}, since the solubility of Ca(OH)$_2$ is 1.65 g L^{-1} in H$_2$O at 20 °C;[38] the flask was sealed with Parafilm laboratory film (Pechiney Plastic Packaging, Bemis Company, Inc., Oshkosh, WI, USA) to avoid carbonatation, and it was vacuum filtered with Whatman quantitative filter paper, grade 40 (Sigma-Aldrich, St. Louis, MO, USA). During the reaction, the solution was mechanically stirred with a four-blade propeller at a rate of 500 min^{-1}. The reactor was placed on a heating plate with automatic temperature control and a precision of ca. 0.5 °C. In addition, 0.2 ± 0.0001 g of the synthetic solid with a particle size of 53-74 μm were used.

The pH was measured in all experiments in the bulk of the solution using an Orion 3-Star pH meter equipped with a Thermo Ultra-Sure flow electrode (Thermo Fisher Scientific, Waltham, MA, USA), which has a reading precision of ca. 0.01 and a range of 0-14 at a maximum temperature of 100 °C. It was also equipped with an automatic temperature compensation (ATC) electrode with an accuracy of 0-100 ± 0.5 °C. To obtain accurate pH measurements,

Table 1. Syntheses conditions of the jarosite-type compounds

	Initial condition / (mol L^{-1})			
	Fe$_2$(SO$_4$)$_3$ nH$_2$O	K$_2$SO$_4$	K$_2$CrO$_4$	Fe(NO$_3$)$_3$ 9H$_2$O
Synthesis 1	0.300	0.300	–	–
Synthesis 2	0.025	0.05	0.2	0.2

the electrode was calibrated with three standards: 4.00 (potassium biphthalate solution), 7.00 (NaH_2PO_4-KH_2PO_4 solution) and 10.01 (H_3BO_3-HCl-NaOH solution) at 25 °C. The slope in all of the calibrations was 96.0 ± 5.0%. The pH meter automatically adjusts the calibration and pH readings to the working temperature. The pH in all the experiments was kept constant by adding small amounts of a concentrated $Ca(OH)_2$ solution. During experiments, either to determine the effect of [OH^-], temperature or particle size effect, one of the variables was modified while the other two were kept constant.

In order to know the progress of the reaction, samples of 5 ± 0.01 mL were taken at different times and then analyzed for K^+ and CrO_4^{2-} by AAS, and SO_4^{2-} by gravimetry. To describe the development of the reaction, the conversion, X, was used. This later, is the mass fraction of the reacting substance and can be calculated according to equation 1:

$$X = \frac{A_t}{A_\tau} \qquad (1)$$

where X is the fraction of the $KFe_3(SO_4)_{2-x}(CrO_4)_x(OH)_6$ solid solution that has reacted; A_t is the amount of K, S or Cr that were released into the solution; and A_τ is the amount of K, S or Cr at the end of the reaction.[39] A number of previous experiments were conducted to select the kinetic model that best describes the behavior of the decomposition reactions. Residual solids were characterized by XRD and SEM-EDS.

Results and Discussion

Synthesis and characterization

Yellow-colored precipitates corresponding to $KFe_3(SO_4)_2(OH)_6$ were obtained in synthesis 1, with a total yield of 85.76 g. The yield of the solid solution $KFe_3(SO_4)_{2-x}(CrO_4)_x(OH)_6$ under the above mentioned conditions was 29.78 g and a reddish-colored precipitate was obtained due to the considerable decrease of SO_4^{2-}. There is also a competition with CrO_4^{2-} for the substitution in the structure. Figures 1a and 1b show particles of $KFe_3(SO_4)_{2-x}(CrO_4)_x(OH)_6$ with a compact spherical morphology, which are composed of soundly joined rhombohedral crystals. Most of crystal have sizes between 1 and 5 μm, but even smaller crystals can be observed. These later, are mainly composed of the jarosite analog $KFe_3(CrO_4)_2(OH)_6$.

Chemical analyses of the solids show that the stoichiometry of the syntheses corresponds to that of jarosite-type compounds. The total percentage of the composition of the solid solution is the following: 6.7% K^+,
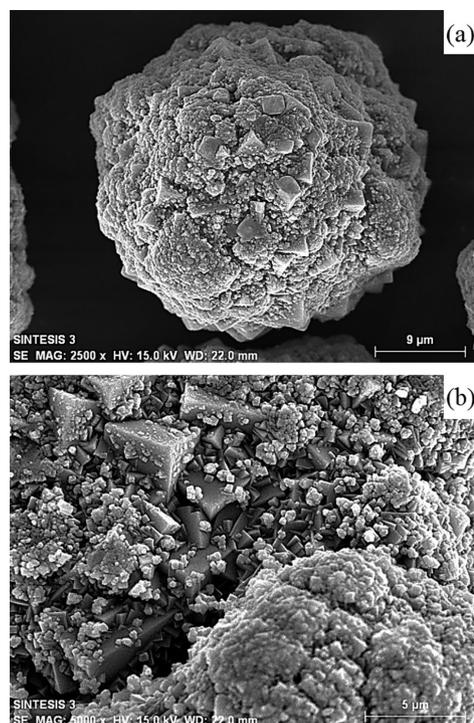
Figure 1. (a) Spherical particle of the obtained precipitates of potassium jarosite with chromium(VI); (b) detailed image of the crystals that constitute the potassium jarosite solid with chromium(VI).

29.88% Fe^{3+}, 27.71% SO_4^{2-}, 17.23% CrO_4^{2-} and 18.48% ($H_3O^+ + OH^- + H_2O$), which was calculated by difference. The approximate formula was obtained from the chemical analysis and it is shown in equation 2:

$$[K_{0.86}(H_3O)_{0.14}]Fe_{2.67}[(SO_4)_{1.23}(CrO_4)_{0.77}][(OH)_{5.01}(H_2O)_{0.99}] \quad (2)$$
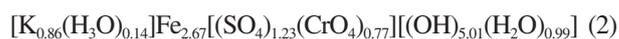
It can be observed that there is a deficiency in K^+, which is attributed to the substitution of the H_3O^+ ion on site A, forming a solid solution between K^+ and H_3O^+, with $K + H_3O = 1$. There is also a deficiency in Fe^{3+} compared to the theoretical formula of jarosite, which is due to the conversion of OH^- ions into H_2O to balance the charge in the structure. This kind of behavior is typical of numerous jarosite-type compounds, both natural and synthetic.[28,36,38-42] Site Z is fully occupied by SO_4^{2-} in the potassium jarosite, but it can be substituted by varying the amount of chromate until it is completely substituted.[43] It was observed that, the larger the radius of the ions that incorporate in the anionic site, the bigger the difficulty to compete with the SO_4^{2-} ion. This is the main limiting factor for the incorporation of a larger amount of CrO_4^{2-} with SO_4^{2-} still present. The general stoichiometry of the synthesis of the solid solution is shown in equation 3:

$$3Fe^{3+} + K^+ + (2 - X)SO_4^{2-} + XCrO_4^{2-} + 6H_2O \rightarrow$$
$$KFe(SO_4)_{2-x}(CrO_4)_x(OH)_6 + 6H^+ \qquad (3)$$
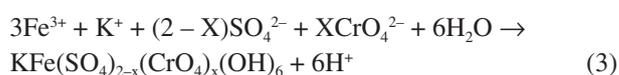
Analysis of the precipitates by XRD (Figure 2a) shows that the peaks obtained in the diffractogram are consistent with those of the Joint Committee on Powder Diffraction Standards (JCPDS; International Centre for Diffraction Data, ICDD) corresponding to the potassium jarosite pattern JCPDS-ICDD.[44] The reflections in both syntheses correspond to jarosite-type compounds $KFe_3(SO_4)_2(OH)_6$. Besides, no additional intensity peaks that may suggest the existence of other crystal phases are observed. The unit cell volume is larger in the solid solution $KFe_3(SO_4)_{2-x}(CrO_4)_x(OH)_6$ than that of synthesis 1, which corresponds to a pure jarosite-type compound. This is due to the fact that chromium(VI) anions have an ionic radius between 0.03225 and 0.05200 nm, while sulfur(VI) anions have an ionic radius between 0.029 and 0.034 nm, which produces thermochemical radii different for each of the two cases (2.4 Å for CrO_4^{2-} and 2.3 Å for SO_4^{2-}). The difference between bond distances makes the XRD peaks shift towards smaller angles. Figure 2b shows the region where the two most intense peaks of potassium jarosite (synthesis 1) and of the solid solution $KFe_3(SO_4)_{2-x}(CrO_4)_x(OH)_6$ (synthesis 2) appear shifted. This change indicates that a solid solution, instead of a two-phase mix, was obtained. Otherwise, different groups of peaks would appear for each phase, which did not happen.[22]
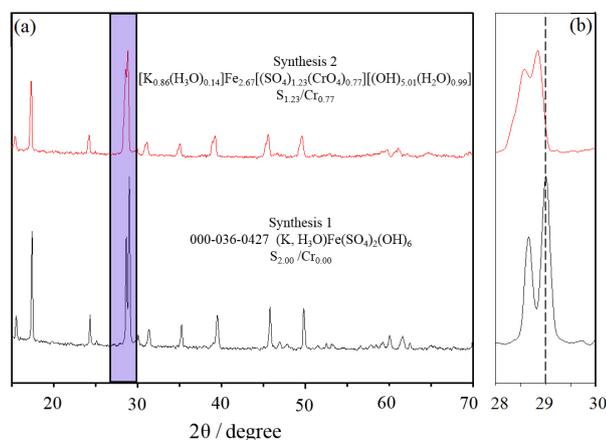
Figure 2. (a) X-ray patterns corresponding to jarosite-type compounds; (b) comparison of the highest intensity peaks of jarosite showing a slight shift.

Nature of the decomposition reaction

In order to determine the nature of the decomposition reaction, samples of the solid solution $KFe_3(SO_4)_{2-x}(CrO_4)_x(OH)_6$ were taken and treated with $Ca(OH)_2$; they were analyzed for K^+ and CrO_4^{2-} by AAS, and for SO_4^{2-} by gravimetry, at different times. The solid residues were characterized by SEM-EDS. The general reaction is composed of three stages: induction period,

progressive conversion period and stabilization period. During the induction period, the particles do not react, and the diffusion of K^+, SO_4^{2-} and CrO_4^{2-} ions is very slow. During this stage, the active centers are formed starting and establishing a reaction front. Anions hydroxide start diffusing through the reaction front from the reaction medium into the particle core. This stage is followed by a progressive conversion period, which is characterized by the formation of a layer of inert products that increases in thickness as the reaction progresses; the core size decreases, as well as the diffusion of K^+, SO_4^{2-} and CrO_4^{2-} ions from the particle core into the reaction medium. The stabilization stage indicates that the reaction has ended, with the concentrations of K^+, SO_4^{2-} and CrO_4^{2-} constant in the solution (Figure 3a).

There are two models in heterogeneous kinetics that can define a chemical reaction: the progressive conversion model and the shrinking core model. The performed experiments are useful for knowing the stage that controls the decomposition reaction and for determining the model that best describes its behavior. In numerous cases, the shrinking core model is the one that best describes the real behavior. Since the resistances of the different stages can be different, the stage controlling the rate is that which presents a higher resistance. In the shrinking core model, there are several stages that control the reaction: diffusion through the fluid film, that surrounds the particle; transport of matter through the layer of inert solids; chemical reaction between the unreacted core interface and the layer of inert products; and a mixed control. The resistance of the fluid film that surrounds the particle can be excluded, because when a layer of inert products is formed, the resistance through it is usually much higher. The following kinetic model (equation 4) describes the reaction when the transport of matter through the layer of inert products is the controlling stage:

$$k_{exp}t = 1 - 2(1 - X) - 3(1 - X)^{2/3} \qquad (4)$$

where X is the fraction of the solid solution that has reacted, k_{exp} is the experimental rate constant and t is the time.[45,46]

If the rate of the chemical reaction is slow compared to that of the transport of matter, equation 5 defines the behavior of the reaction:

$$k_{exp}t = 1 - (1 - X)^{1/3} \qquad (5)$$

In order to prove which of the two equations describes better the actual behavior, experiments were conducted at constant [OH^-], T and d_0 and the solid conversion was determined at different times. A representation of equations 4 and 5 that are function of X_K, fraction of

potassium in solution against of time should be linear. The slope of any of the equations is k_{exp}, while the intersection with t represents the induction time (t_{ind}), which represents the duration of the induction period.

Figure 3a shows the progress of a decomposition reaction for K, Cr and S. On the other hand, Figure 3b presents a comparison between equations 4 and 5 applied to the performed experiments. The shrinking core model with chemical control (equation 5) is the one that best describes the actual behavior of the decomposition reaction of the solid $KFe_3(SO_4)_{2-x}(CrO_4)_x(OH)_6$. Since the difference in the linear regression coefficient for both models is not quite considerable, there can be no doubt that chemical control is the one that rules the global kinetics. However, in the control by transport, the order of reaction is always n = 1.0, the reaction rate depends little on temperature and it is sensitive to the stirring rate. On the other hand, when the chemical reaction is the controlling stage, the chemical rate constant is independent from the hydrodynamics and very sensitive to temperature, the order of reaction is different from n = 1.0; it is also independent from the formation or non-formation of layers of inert product.[47] For such reasons, it can be established that the shrinking core model with chemical control is the one that describes the decomposition reaction.
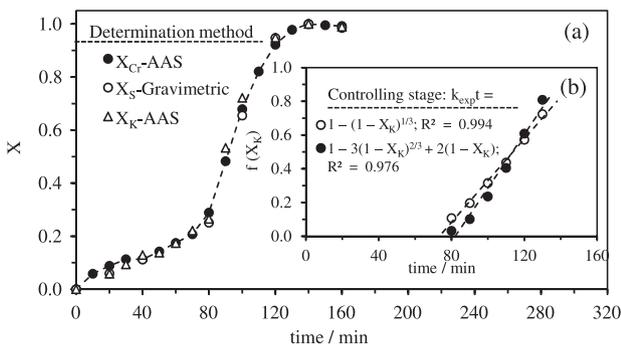
Figure 3. (a) Decomposition curve of the solid $KFe_3(SO_4)_{2-x}(CrO_4)_x(OH)_6$; (b) comparison between the shrinking core model by transport of matter and the shrinking core model with chemical control. X_S, X_K and X_{Cr} are the sulfur, potassium and chromium fractions in solution, respectively; AAS: atomic absorption spectrometry. Experimental conditions: $[Ca(OH)_2] = 1.4$ g L^{-1}, temperature = 30 °C, particle size (d_0) = 53-74 µm, 500 min^{-1}.

The experimental rate constant is thus expressed by equation 6:

$$k_{exp} = \frac{b\,k_q C_A^n}{\rho_B r_0} \qquad (6)$$

where b is a stoichiometric coefficient, k_q is the chemical rate constant, C_A is the reactant concentration, n is the order of reaction, ρ_B is the density of the reacting solid, and r_0 is the initial particle radius. The density of the

solid was calculated with a 25 mL Brand pycnometer (Brand GMBH + CO KG, Wertheim, Germany) using distilled water as immersion liquid. The result was 2880 kg m^{-3}.

Figure 4a shows a partially decomposed particle where a layer of solid residues, formed by the partial reaction of jarosite, can be observed; it is followed by a reaction front and an unreacted core. EDS analysis (Figures 4b and 4c) shows the presence of Cr, K, S, Fe and O in the particle core, which confirms that it has not reacted. The five analyzed elements can also be observed in the layer of solid residues. However, only Fe, Cr and O remain near the initial concentration, while the intensity peaks of K and S decrease drastically in the layer of solid residues, as they have diffused in larger proportion into the solution.
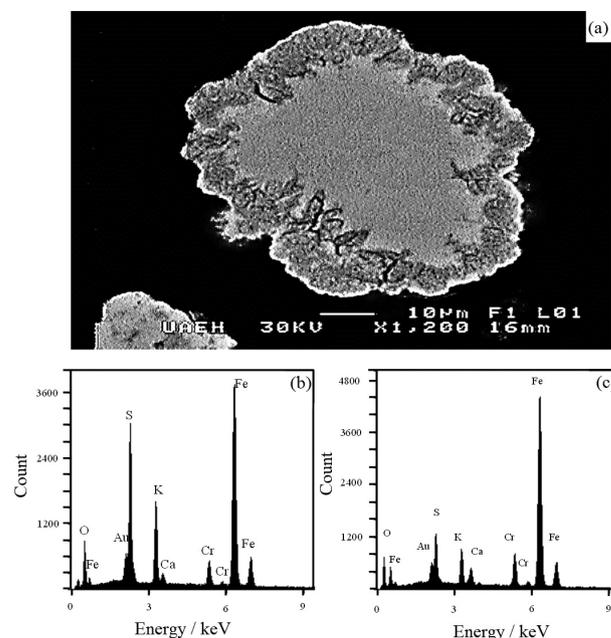
Figure 4. (a) Partially decomposed particle of the solid solution $KFe_3(SO_4)_{2-x}(CrO_4)_x(OH)_6$, x = 0.8, backscattered electrons; (b) energy dispersive X-ray spectrometer (EDS) spectra corresponding to the unreacted core; (c) layer of solid residues. Experimental conditions: $[Ca(OH)_2] = 1.4$ g L^{-1}, temperature = 30 °C, particle size (d_0) = 53-74 µm, 500 min^{-1}.

EDS linear scanning (Figure 5a) from the core to the layer of solid residues shows a uniform amount of K, Cr, S and Fe in the core, followed by a decrease in K and S, and a Fe increase in the solid residues. The amount of Cr remains constant because one part is adsorbed and retained in the reacted particle. Although one would think that S and Cr proportionally diffuse from the core into the solution, Cr diffuses in a much smaller proportion compared to S due to the similarity of their thermochemical radii. In some particles, the outline of the unreacted core may not be perfectly defined, as is the case with the particle used for

this scanning. However, the shrinking core model with chemical control describes the behavior of the reaction fairly well. In order to confirm the previously described results, one partially decomposed particle was subject to a mapping of the different elements that constitute the solid KFe$_3$(SO$_4$)$_{2-x}$(CrO$_4$)$_x$(OH)$_6$ (Figure 5b).
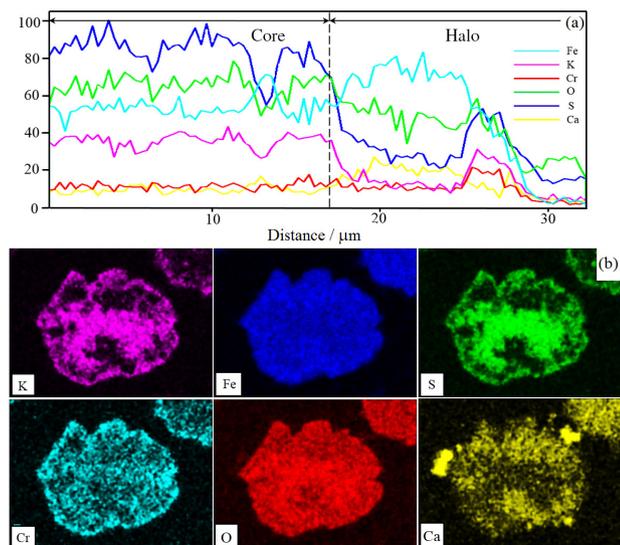
Figure 5. (a) Linear scanning of the particle in Figure 4b; (b) mapping of a partially decomposed particle for K, Fe, S, Cr, O and Ca. Experimental conditions: [Ca(OH)$_2$] = 1.4 g L^{-1}, temperature = 30 °C, particle size (d$_0$) = 53-74 μm, 500 min^{-1}.

It can be observed that Fe and O are distributed evenly throughout the particle, and K and S can be seen in greater proportion in the unreacted core. In a larger proportion compared to K and S, Cr is observed through the core and the layer of solid residues. It is worth noting that the reaction happens along a diffused front instead of a clear surface between the unreacted solid and the ash. Although Levenspiel[45] mentions that this kind of behavior is a middle point between the shrinking core model and the progressive conversion model, the experiments are better described by the shrinking core model. In addition, it is noteworthy that the presence of Ca adhered to the particle due to the formation of CaCO$_3$ during the reaction, which complicated the creation of active points and the diffusion of OH$^-$ ions into the particle core. In this case, there is no proper diffusion of OH$^-$ ions into the interface between the ash layer and the unreacted core.[38,46]

X-ray diffraction analysis shows the gradual decomposition of the synthetic solid, which becomes amorphous at a reaction time of 140 min and a concentration of Ca(OH) = 1.4 g L^{-1} are shown in Figure 6. The residual solid is most probably composed of iron hydroxide with weakly adsorbed CrO$_4^{2-}$. No formation of new phases with compositions different from the initial solids was observed. The solids analyzed at 140 min show slight intensity

diffraction peaks corresponding to CaCO$_3$ in 2θ = 28°. This kind of behavior is similar to that previously studied in synthetic jarosites.[29,32,35,48]
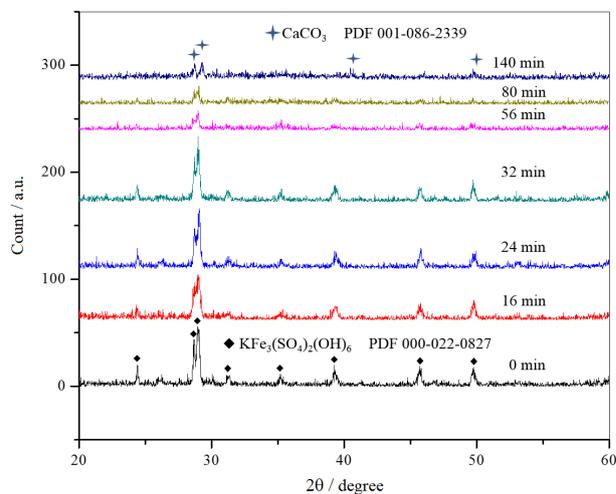
Figure 6. Diffractograms obtained from the solid KFe$_3$(SO$_4$)$_{2-x}$(CrO$_4$)$_x$(OH)$_6$ at different reaction times showing a gradual decrease in the diffraction peaks intensities with increments in time. Experimental conditions: [Ca(OH)$_2$] = 1.4 g L^{-1}, temperature = 30 °C, particle size (d$_0$) = 53-74 μm, 500 min^{-1}.

Decomposition reactions are usually stoichiometric, but in this case the reaction is incongruous, as the molar fractions do not coincide with the conducted calculations. The molar fraction of K$^+$ and SO$_4^{2-}$ in aqueous solution is very close to the molar fraction in solids. However, there is a slight difference in the case of Cr. The formation of an amorphous iron hydroxide with CrO$_4^{2-}$ weakly adsorbed at the end of the reaction is proposed, since the attraction forces towards SO$_4^{2-}$ are probably weaker than those of CrO$_4^{2-}$, thus allowing the presence of a larger amount of Cr. Therefore, the decomposition reaction is expressed by equation 7:

$$[K_{0.86}(H_3O)_{0.14}]Fe_{2.67}[(SO_4)_{1.23}(CrO_4)_{0.77}][(OH)_{5.01}(H_2O)_{0.99}]_{(s)} + 3.14OH^-_{(aq)} \rightarrow 0.86K^+_{(aq)} + 1.23SO_4^{2-}_{(aq)} + xCrO_4^{2-}_{(aq)} + 2.67Fe(OH)_3 \cdot yCrO_4^{2-}_{(s)} + 1.27H_2O_{(l)}, \; x + y = 0.77 \qquad (7)$$
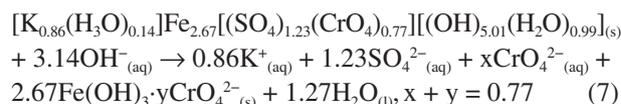
Dependence of the induction and progressive conversion period

Figures 7, 8 and 9 show the decomposition curves for the effects of [OH$^-$], T and d$_0$, respectively, as well as the plots of the shrinking core model with chemical control for each corresponding effect. All the reactions were monitored by potassium leaching, as k$_{exp}$ is identical for K, Cr or S (Figures 3a and 3b), and thus, there is no change in the reaction rate.

Then, k$_{exp}$ and t$_{ind}$ were determined in order to calculate the order of reaction and activation energy in each case.
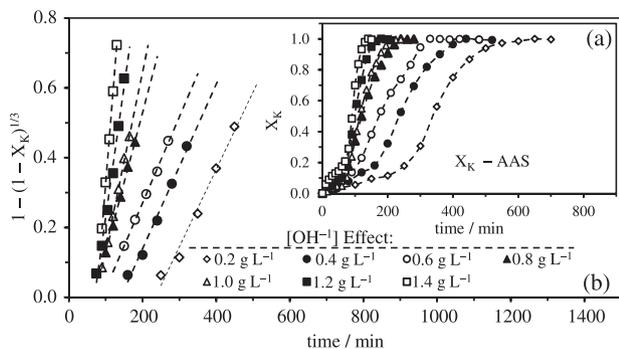
Figure 7. (a) Decomposition curves in Ca(OH)$_2$ medium, [OH$^-$] effect; (b) chemical control model with formation of a layer of solid products. Conditions: temperature = 30 °C, particle size (d$_0$) = 53-74 μm, 500 min^{-1}.
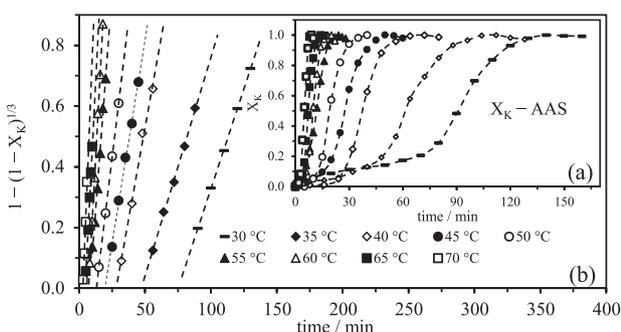
Figure 8. (a) Decomposition curves in Ca(OH)$_2$ medium, temperature effect; (b) chemical control model with formation of a layer of solid products. Conditions: [Ca(OH)$_2$] = 1.4 g L^{-1}, particle size (d$_0$) = 53-74 μm, 500 min^{-1}.
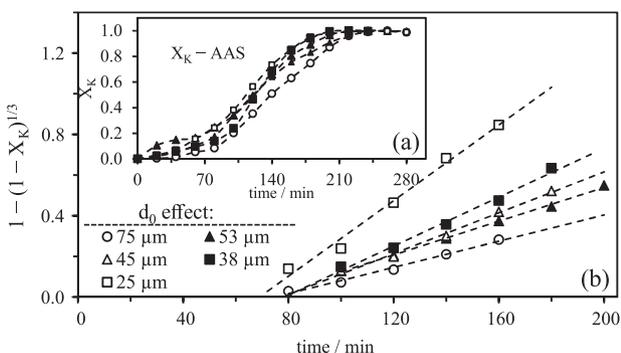
Figure 9. (a) Decomposition curves in Ca(OH)$_2$ medium, particle size effect; (b) chemical control model with formation of a layer of solid products. Conditions: [Ca(OH)$_2$] = 0.8 g L^{-1}, temperature = 30 °C, 500 min^{-1}.

If logarithms are applied to equation 7, equation 8 is obtained:

$$\log k_{exp} = \log \frac{bk_q}{\rho_B r_0} + n \log C_A \qquad (8)$$

By plotting the values of the logarithm of k_{exp} as a function of the logarithm of C_A ([OH$^-$]), a straight line is obtained where the slope represents the order of

reaction n (Figure 10a). For the progressive conversion period, at [OH$^-$] ≥ 0.0206 mol L^{-1}, the order of reaction is n = 1.99 with respect to OH$^-$, which indicates that at those conditions the reaction strongly depends on concentration. For [OH$^-$] ≤ 0.0206 mol L^{-1}, the order of reaction is n = 0 with respect to OH$^-$, and under these conditions there is no dependence on [OH$^-$] that causes a change in the reaction mechanism. Elwood Madden *et al.*[49] proved that the dissolution of potassium is dependent on pH, with a minimum rate that occurs at approximately pH 3.5. It was suggested that two dissolution mechanisms can occur: at pH < 3.5 the H$^+$ attack is the dominating mechanism, while at pH > 3.5 the OH$^-$ attack is the controlling mechanism. Kendall *et al.*[43] suggested a third mechanism for the dissolution rates of jarosites with arsenic. They propose that near the point of zero charge of the jarosite, the dissolution may be controlled by water attack. Flores *et al.*[48] and Reyes *et al.*[50] found orders of reaction of n = 0 at low [OH$^-$], which is indicative of inexistent dependence on the reaction medium. In the present work, it is proposed that when there is no dependence on the reaction medium [OH$^-$], the attack towards the solid particles is done by water,[43] which results in orders of reaction equal to zero and, therefore, much slower reaction rates independent of [OH$^-$].

The dependence of the chemical rate constant on temperature is given by equation 9 (Arrhenius equation):

$$k_q = k_0 e^{(-E_a/RT)} \qquad (9)$$

where k_0 is the frequency factor, E_a is the activation energy, R is 8.3144 J mol^{-1} K^{-1} and T is temperature in Kelvin. By substituting the chemical rate constant in the previous equation, arranging factors and applying natural logarithm, the following equation is obtained (equation 10):

$$\ln \frac{k_{exp}}{[OH^-]^n} = \ln \frac{2\bar{v}k_0}{d_0} - \frac{E_a}{R}\left(\frac{1}{T}\right) \qquad (10)$$

When plotting $\ln k_{exp}/[OH]^n$ against 1/T, a straight line, where m = $-E_a/R$, is obtained; it allows to calculate the activation energy. Thus, for the progressive conversion period, an E_a = 51.56 kJ mol^{-1} was obtained (Figure 10b).

The dependence of induction time on concentration was calculated in a similar manner. By plotting [OH$^-$] against t_{ind}, Figure 11a is obtained, where it can be noticed that when [OH$^-$] decreases, the induction time increases, while at high OH$^-$ concentrations the induction time remains constant. A possible explanation for this is that in this reaction medium, a layer of CaCO$_3$ is formed, thus blocking the diffusion of OH$^-$ ions into the surface and delaying the formation of active points for the creation of a reaction
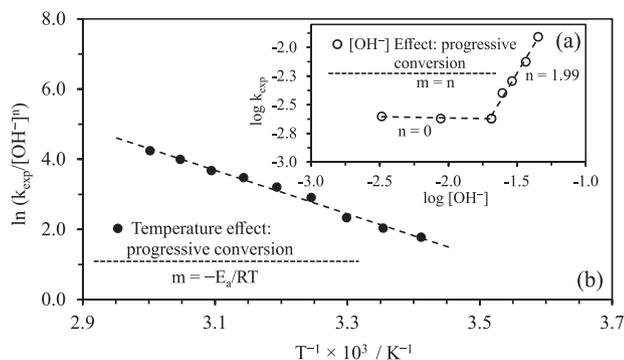
Figure. 10. (a) Plot to determine the orders of reaction by equation 8; (b) activation energy determined by equation 10.

front. Figure 11b shows the log [OH$^-$] against log (t$_{ind}^{-1}$) for the dependence of [OH$^-$] with respect to induction time. At [OH$^-$] $\leq$ 0.0248 mol L^{-1}, there are no perceptible effects on the induction period due to the previously stated reasons. At [OH$^-$] $\geq$ 0.0248 mol L^{-1} there is an order of reaction n = 0.62 with respect to OH$^-$. All of the obtained kinetic parameters for both periods are summarized in Table 2.
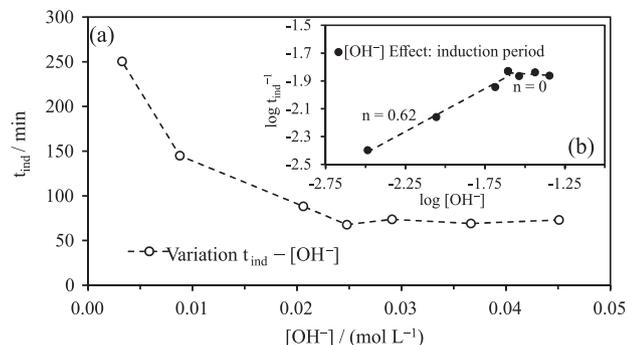
Figure. 11. (a) Plot of induction time (t$_{ind}$) *vs.* OH$^-$ concentration; (b) dependence of t$_{ind}$ with respect to OH$^-$ concentration to calculate the order of reaction.

Table 2. Kinetic parameters calculated in the dissolution experiments of KFe$_3$[(SO$_4$)$_{2-x}$(CrO$_4$)$_x$](OH)$_6$ in medium Ca(OH)$_2$ for induction and conversion periods

Kinetic parameter	Induction period	Progressive conversion period
E$_a$ / (J mol^{-1})	63750	51560
n	0.62	1.99
V$_m$k$_0$r$_0^{-1}$	3.27 × 10^9	8.915 × 10^9

E$_a$: Activation energy; k$_0$: frequency factor; r$_0$: initial particle radius.

Kinetic modeling

Figure 12a shows the dependence of k$_{exp}$ with respect to initial particle diameter. As it can be observed, the experimental constant is inversely proportional to particle diameter (k$_{exp}$ α 1 / d$_0$) Therefore, the decomposition of the solid solution KFe$_3$(SO$_4$)$_{2-x}$(CrO$_4$)$_x$(OH)$_6$ is described by the

shrinking core model with chemical control and the particle size has no significant effect on the induction period.
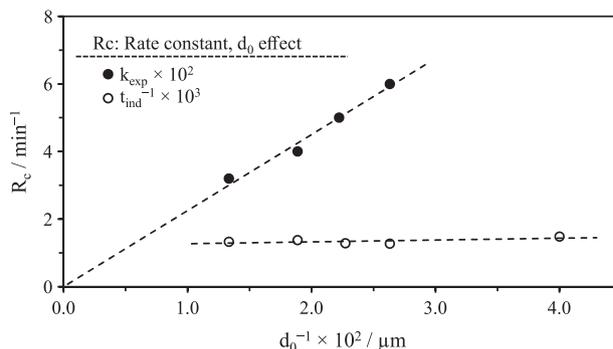
Figure. 12. Plot of the dependence of experimental rate constant (k$_{exp}$) and induction time (t$_{ind}^{-1}$) with respect to particle size (d$_0$).

The activation energy in the induction period is determined from the slope of the straight line obtained by plotting log t$_{ind}^{-1}$ *vs.* 1/T. The activation energy corresponding to the induction period is E$_a$ = 63.75 kJ mol^{-1} (Figure 13a). It can be seen in this stage that the induction period decreases as temperature is increased (Figure 13b). The activation energy values are consistent with those determined for a chemical control: 40 kJ mol^{-1}.[47] The increase of the activation energy in the induction period is related to the fact that in the initial stage of the reaction a larger amount of energy is needed due to the difficulty of OH$^-$ ions to get through the CaCO$_3$ layer and subsequently form the active centers where the reaction is started; once they are formed, the reaction occurs faster.
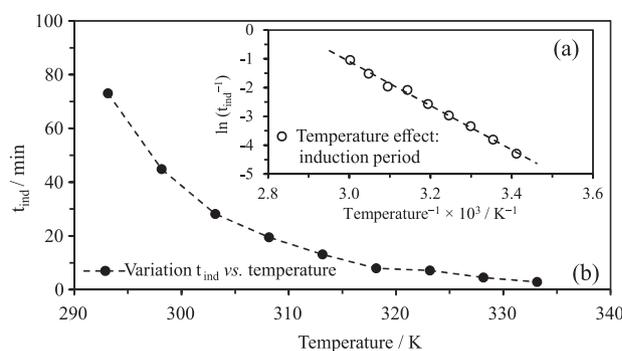
Figure. 13. (a) Plot of the dependence of induction time (t$_{ind}$) with respect to temperature for the decomposition of the solid KFe$_3$(SO$_4$)$_{2-x}$(CrO$_4$)$_x$(OH)$_6$; (b) relationship between t$_{ind}$ and temperature.

Table 3 shows the processing conditions as well as the experimental data obtained from dissolution experiments.

Concentration of OH$^-$ was determined by taking into account the pH in each experiment, as well as the ionization constant of water for each working temperature.[39,47,51] A

Table 3. Conditions and experimental results of the dissolution of $KFe_3[(SO_4)_{2-x}(CrO_4)_x](OH)_6$ in $Ca(OH)_2$ medium

pH	[OH⁻] / (mol L⁻¹)	Temperature / K	d_0 / μm	Stirring / min⁻¹	t_{ind} / min	k_{exp} / min⁻¹	Total reaction time / min
12.49	0.0451	303	53	500	73.04	0.0124	140
12.40	0.0366	303	53	500	69.08	0.0075	180
12.30	0.0291	303	53	500	73.56	0.0051	210
12.23	0.0248	303	53	500	67.8	0.0040	240
12.15	0.0206	303	53	500	88.13	0.0024	330
11.78	0.0088	303	53	500	144.83	0.0024	440
11.35	0.0033	303	53	500	250.28	0.0025	650
12.30	0.0410	308	53	500	44.82	0.0134	112
12.22	0.0480	313	53	500	28.12	0.0241	72
11.98	0.0380	318	53	500	19.45	0.0268	50
11.85	0.0380	323	53	500	13.09	0.0361	40
11.77	0.0410	328	53	500	7.98	0.0573	24
11.68	0.0440	333	53	500	7.11	0.0798	20
11.51	0.0390	338	53	500	4.53	0.0846	14
11.4	0.0390	343	53	500	2.83	0.1070	9
12.25	0.0260	303	75	500	75.46	0.0032	260
12.26	0.0260	303	45	500	78.00	0.0050	220
12.30	0.0290	303	38	500	78.68	0.0060	240
12.21	0.0230	303	25	500	67.36	0.0093	220

general kinetic model is presented in equation 11, which is obtained by substituting and arranging equations 6, 7 and 9, and by using the kinetic parameters shown in Table 3:

$$[1 - (1 - x)^{1/3}] = \frac{bk_0}{\rho_B r_0} e^{E_a/RT} [OH^-]^n t \tag{11}$$

The kinetic expression in the induction period is shown in equation 12:

$$\frac{1}{t_{ind}} = 1.130 \times 10^{10} \, e^{-63750/RT} [OH^-]^{0.62} \tag{12}$$

For the progressive conversion period, the resulting kinetic expression is shown in equation 13:

$$[1 - (1 - X_k)^{1/3}] = 3.915 \times 10^9 \, e^{-51560/RT} [OH^-]^{1.99} t \tag{13}$$

The plot of the logarithm of the reaction rates constants (R_c) against the logarithm of the of the experimental values was obtained from equations 12 and 13 for every kinetic stage (k_{exp}, t_{ind}^{-1}; Figure 14a). It can be noticed in this figure that the values of the equations for the induction and progressive conversion period are satisfactorily consistent with the experimental values. In addition, it is possible to obtain a new expression to determine the

necessary time for any conversion of the solid solution $KFe_3(SO_4)_{2-x}(CrO_4)_x(OH)_6$ in $Ca(OH)_2$ medium, which is described in equation 14:

$$t = \frac{1}{\dfrac{r_0}{V_m}(3.27 \times 10^9) \, e^{(-63.750/RT)} [OH^-]^{0.62}} + \frac{[1 - (1 - x)^{1/3}}{(8.915 \times 10^9) \, e^{(-51.560/RT)} [OH^-]^{1.99}} \tag{14}$$

Figure 14b shows the necessary reaction time to obtain a conversion of X = 0.75 by taking into account the data obtained for each of the experiments. The experimental values are consistent with the obtained model for any conversion at any given time.

It is observed that for the progressive conversion period in $Ca(OH)_2$ medium, the reaction depends more on [OH⁻] than on the other variables. This behavior is related to the adsorption difficulty of OH⁻ ions in the $KFe_3(SO_4)_{2-x}(CrO_4)_x(OH)_6$ particles. In this case, there is no proper diffusion of OH⁻ ions into the interface between the ash layer and the unreacted core. This happens because $CaCO_3$ blocks the particles' pores. It can be confirmed through the order of reaction obtained for the progressive conversion period (n = 1.99), which is higher than that obtained in the induction period (n = 0.69). There is a strong relation
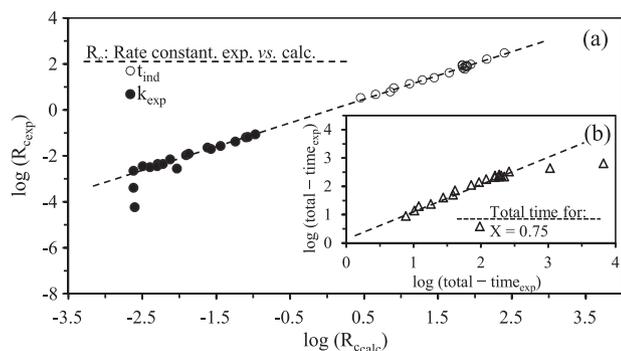
Figure. 14. (a) Comparison plot of the calculated and experimental rate constants (k$_{exp}$) for the induction (t$_{ind}$) and progressive conversion period; (b) plot of the kinetic modeling of reaction time needed to produce a conversion of X = 0.75; experimental values *vs.* calculated values.

between the temperature of reaction and [OH$^-$], given by the ionization constant of water, which indicates that at high temperatures, pH decreases and consequently OH$^-$ concentration also decreases. For this reason, the [OH$^-$] *vs.* temperature interaction has a strong influence on the decomposition process. The behavior of the reaction and experimental data are satisfactorily consistent with the established kinetic models, which involves the induction and progressive conversion periods, as well as the total time of reaction for all the experiments. These models are capable of predicting the behavior of this kind of compound under the studied conditions. However, they will only apply for the used reaction medium. Previous works on the decomposition of jarosites in Ca(OH)$_2$ medium have had similar results.[39,46,47,50]

Conclusions

The synthesis of potassium jarosite with chromium(VI) leads to the formation of a solid solution with the following formula: [K$_{0.86}$(H$_3$O)$_{0.14}$]Fe$_{2.67}$(SO$_4$)$_{1.23}$(CrO$_4$)$_{0.77}$[(OH)$_{5.01}$ (H$_2$O)$_{0.99}$]. The decomposition of the solid solution KFe$_3$(SO$_4$)$_{2-x}$(CrO$_4$)$_x$(OH)$_6$ in Ca(OH)$_2$ medium is consistent with the shrinking core model with chemical control and characterized by two main stages: an induction period and a progressive conversion period.

The induction period decreases when both the OH$^-$ concentration and temperature increase, and particle size does not have an important influence. The dependence on temperature is very significant, and t$_{ind}$ tends to zero with increments in temperature, while the maximum dependence on [OH$^-$] is reached at [OH$^-$] = 0.0248 mol L^{-1}, with an order of reaction of n = 0.62 with respect to OH$^-$ and an E$_a$ = 63.75 kJ mol^{-1}.

The progressive conversion period is characterized by the formation of a reaction front around an unreacted

core; and there is a diffusion of ions of site A (K$^+$), site Z [sulfur(VI) and chromium(VI)], from the crystal lattice, through the layer of solid residues (made of iron hydroxides with weakly adsorbed chromate) towards the solution. In this stage at [OH$^-$] $\geq$ 0.0206 mol L^{-1}, the order of reaction is n = 1.99 with respect to OH$^-$; and for [OH$^-$] $\leq$ 0.0206 mol L^{-1}, the order of reaction is n = 0 with respect to OH$^-$; the activation energy in this stage is E$_a$ = 51.56 kJ mol^{-1}.

The decomposition rate is faster for smaller initial particle size, according to the relationship k$_{exp}$ α 1/d$_0$.

At room temperature conditions (303 K) and low OH$^-$ concentrations, chromium(VI) is retained in the porous surface of the residue, which makes it convenient for avoiding the transport of chromium(VI) into natural effluents. Since the amount of released chromate during the reaction is less compared to that of sulfate, it can be concluded that potassium jarosite is ideal for retaining amounts of chromium contained in effluents without being released into the environment, even if it reacts in environments of extreme alkalinity.

Since it is difficult to find environments of extreme alkalinity (such as the working conditions presented in this piece of work) in nature, it is possible to use jarosite as a material to reservoir chromium(VI), as long as extended exposition times and high temperatures are avoided, as conditions that appear after a lime treatment process.

Acknowledgments

References

1. Hemalatha, P.; Prasada Rao, P. V. V.; *Int. J. Environ. Sci.* **2012**, *2*, 2321.

2. Lee, T.; Lim, H.; Lee, Y.; Park, J. W.; *Chemosphere* **2003**, *53*, 479.

3. Guan, X.; Dong, H.; Ma, J.; Lo, I. M. C.; Dou, X.; *Sep. Purif. Technol.* **2011**, *80*, 179.

4. Guertin, J.; Jacobs, J. A.; Avakian, C. P.; *Chromium(VI) Handbook*, 1st ed.; CRC Press: USA, 2005.

5. Baron, D.; Palmer, C. D.; *Geochim. Cosmochim. Acta* **2002**, *66*, 2841.

6. Anandkumar, J.; Mandal, B.; *J. Hazard Mater.* **2011**, *186*, 1088.

7. Park, D.; Ahn, C. K.; Kim, Y. M.; Yun, Y. S.; Park, J. M.; *J. Hazard. Mater.* **2008**, *160*, 422.

8. Park, D.; Yun, Y. S.; Lee, H. W.; Park, J. M.; *Bioresour. Technol.* **2008**, *99*, 1141.

9. Somasundaram, V.; Philip, L.; Bhallamudi, S. M.; *J. Hazard. Mater.* **2009**, *172*, 606.

10. Martins, M.; Faleiro, M. L.; Chaves, S.; Tenreiro, R.; Santos, E.; Costa, M. C.; *J. Hazard. Mater.* **2010**, *176*, 1065.

11. Rajeshwari, K.; Kumar, M. S.; Thajuddin, N.; *Ann. Microbiol. (Heidelberg, Ger.)* **2012**, *62*, 241.

12. Castro, L.; García-Balboa, C.; González, F.; Ballester, A.; Blázquez, M. L.; Muñoz, J. A.; *Hydrometallurgy* **2013**, *131-132*, 29.

13. Wang, S. L.; Chen, C. C.; Tzou, Y. M.; Hsu, C. L.; Chen, J. H.; Lin, C. F.; *J. Hazard. Mater.* **2009**, *164*, 223.

14. Fiol, N.; Escudero, C.; Villaescusa, I.; *Bioresour. Technol.* **2008**, *99*, 5030.

15. Hunsom, M.; Pruksathorn, K.; Damronglerd, S.; Vergnes, H.; Duverneuil, P.; *Water Res.* **2005**, *39*, 610.

16. Asta, M. P.; Cama, J.; Martínez, M.; Giménez, J.; *J. Hazard. Mater.* **2009**, *171*, 965.

17. Welch, S. A.; Christy, A. G.; Kirste, D.; Beavis, S. G.; Beavis, F.; *Chem. Geol.* **2007**, *245*, 183.

18. Jambor, J. L.; *Can. Mineral.* **1999**, *37*, 1323.

19. Dutrizac, J. E.; *Metall. Mater. Trans. B* **2008**, *39B*, 771.

20. Dutrizac, J. E.; Chen, T. T.; *Hydrometallurgy* **2009**, *98*, 128.

21. Basciano, L. C.; Peterson, R. C.; *Am. Mineral.* **2007**, *92*, 1464.

22. Baron, D.; Palmer, C. D.; *Geochim. Cosmochim. Acta* **1996**, *60*, 3815.

23. Paktunc, D.; Dutrizac, J. E.; *Can. Mineral.* **2003**, *41*, 905.

24. Savage, K. S.; Bird, D. K.; O'Day, P. A.; *Chem. Geol.* **2005**, *215*, 473.

25. Dutrizac, J. E.; Chen, T. T.; *Hydrometallurgy* **2010**, *102*, 55.

26. Dutrizac, J. E.; Kaiman, S.; *Hydrometallurgy* **1975**, *1*, 51.

27. Forray, F. L.; Smith, A. M. L.; Drouet, C.; Navrotsky, A.; Wright, K.; Hudson-Edwards, K. A.; Dubbin, W. E.; *Geochim. Cosmochim. Acta* **2010**, *74*, 215.

28. Johnson, D. B.; Hallberg, K. B.; *Sci. Total Environ.* **2005**, *338*, 3.

29. Liu, F.; Zhou, J.; Zhou, L.; Zhang, S.; Liu, L.; Wang, M.; *J. Hazard. Mater.* **2015**, *299*, 404.

30. Zahrai, S. K.; Elwood Maden, M. E.; Maden, A. S.; Rimstidt, J. D.; *Icarus* **2013**, *223*, 438.

31. Patiño, F.; Viñals, J.; Roca, A.; Nuñez, C.; *Hydrometallurgy* **1994**, *34*, 279.

32. Patiño, F.; Salinas, E.; Cruells, M.; Roca, A.; *Hydrometallurgy* **1998**, *49*, 323.

33. Patiño, F.; Cruells, M.; Roca, A.; Salinas, E.; Perez, M.; *Hydrometallurgy* **2003**, *70*, 153.

34. Cruells, M.; Roca, A.; Patiño, F.; Salinas, E.; Rivera, I.; *Hydrometallurgy* **2000**, *55*, 153.

35. Roca, A.; Patiño, F.; Viñals, J.; Nuñez, C.; *Hydrometallurgy* **1993**, *33*, 341.

36. Roca, A.; Cruells, M.; Patiño, F.; Rivera, I.; Plata, M.; *Hydrometallurgy* **2006**, *81*, 15.

37. ASTM Committee E-29; *Manual on Test Sieving Methods*; American Society for Testing and Materials: Philadelphia, 1985.

38. Maloney, J. O.; *Perry's Chemical Engineers' Handbook*, 8th ed.; McGraw-Hill: New York, 2008.

39. Patiño, F.; Reyes, I. A.; Flores, M. U.; Pandiyan, T.; Roca, A.; Reyes, M.; Hernández, J.; *Hydrometallurgy* **2013**, *137*, 115.

40. Dutrizac, J. E.; Kayman, S.; *Can. Mineral.* **1976**, *14*, 151.

41. Dutrizac, J. E.; *Metall. Mater. Trans. B* **1983**, *14*, 531.

42. Dutrizac, J. E.; Jambor, J. L.; Chen, T. T.; *Can. Met.* **1987**, *26*, 103.

43. Kendall, M. R.; Madden, A. S.; Elwood Madden, M. E.; Hu, Q.; *Geochim. Cosmochim. Acta* **2013**, *112*, 192.

44. The Plessey Company Limited; International Centre for Diffraction Data; Jarosite, syn pattern: PDF 00-022-0827.

45. Levenspiel, O.; *Ingeniería de las Reacciones Químicas*, 3ª ed.; Reverté: Barcelona, 2010.

46. Patiño, F.; Flores, M. U.; Reyes, I. A.; Reyes, M.; Hernández, J.; Rivera, I.; Juárez, J. C.; *Geochem. T.* **2013**, *14:2*, 1.

47. Ballester, A.; Verdeja, L. F.; Sancho, J.; *Metalurgia Extractiva Fundamentos (Vol. 1)*, 1ª ed.; Síntesis: Madrid, 2000.

48. Flores, M. U.; Patiño, F.; Reyes, I. A.; Rivera, I.; Reyes, M.; Juárez, J. C.; *J. Braz. Chem. Soc.* **2012**, *6*, 1018.

49. Elwood Madden, M. E.; Madden, A. S.; Rimstidt, J. D.; Zaharai, S.; Kendall, M. R.; Miller, M. A.; *Geochim. Cosmochim. Acta* **2012**, *91*, 306.

50. Reyes, I. A.; Patiño, F.; Rivera, I.; Flores, M. U.; Reyes, M.; Hernández, J.; *J. Braz. Chem. Soc.* **2011**, *12*, 1260 .

51. Lide, D. R.; *Handbook of Chemistry and Physics*, 94th ed.; CRC Press: Boston, 2009.